ADVANCED FUNCTIONAL MATERIALS
www.afm-journal.de

Functionalization of Nanostructured Hematite Thin-Film Electrodes with the Light-Harvesting Membrane Protein C-Phycocyanin Yields an Enhanced Photocurrent

Debajeet K. Bora, Elena A. Rozhkova, Krisztina Schrantz, Pradeep P. Wyss, Artur Braun, Thomas Graule, and Edwin C. Constable*

The integration of light-harvesting proteins and other photosynthetic molecular machinery with semiconductor surfaces plays an important role in improving their performance as solar-cell materials. Phycocyanin is one such protein that can be employed for this purpose. Phycocyanins have light-harvesting properties and belong to the phycobilisome protein family. They are present in cyanobacteria, which capture light energy and funnel it to reaction centers during photosynthesis. Here, a way of increasing the photocurrent of hematite by covalent cross-coupling with phycocyanin is reported. For this, a hematite–phycocyanin integrated system is assembled by consecutive adsorption and cross-coupling of protein molecules, separated by an agarose layer and a linker molecule, on the top of a mesoporous hematite film. The hematite–phycocyanin assembly shows a two-fold increased photocurrent in comparison with pristine hematite film. The increase in the photocurrent is attributed to the enhanced light absorption of the hematite film after integration with the protein, as is evident from the UV–vis spectra and from the photocurrent-action spectrum. The assembly shows long-term stability and thus constitutes a promising hybrid photoanode for photo-electrochemical applications.

1. Introduction

Light harvesting is the initial step in the photosynthesis of plants and cyanobacteria, followed by the splitting of water and the formation of O_2 by the photosystem II.[1] Nature thus provides an early model of light absorption and charge-separation structures that can drive fuel-forming photochemical reactions. The inorganic analog of this process is photo-electrochemical water-splitting on semiconductor electrodes.[2] Effort has been made to mimic nature by "artificial photosynthesis," such as by integration of light-harvesting-protein complexes with inanimate, inorganic material with photovoltaic properties.[3] The charge transfer across protein/solid-state junctions has been identified as an important matter in this respect.[4] The integration of the light-harvesting complex 2 (LH2 complex) from *Rhodobacter sphaeroides* to patterned self-assembled monolayers at the micrometer scale has been demonstrated.[5] This approach is an interesting application in the area of biomimetic photovoltaic devices,[6] taking advantage of the interaction of metalloproteins with oxide semiconductors. Another biomimetic light-harvesting-device concept has been developed using the interaction of a cellular organelle, such as a chlorosome, with TiO_2.[7] A biomimetic photonic-energy-conversion system was developed by immobilizing the photoactive protein-complex photosystem I on the surface of nanoporous gold electrodes, so as to drive a photoinduced electric current through an electrochemical cell.[8] A detailed study of

D. K. Bora, Dr. K. Schrantz, P. P. Wyss, Dr. A. Braun, Prof. T. Graule
Laboratory for High Performance Ceramics
Empa. Swiss Federal Laboratories for Materials Science and Technology
Überlandstrasse 129, CH-8600 Dübendorf, Switzerland
E-mail: artur.braun@alumni.ethz.ch

D. K. Bora, Prof. E. C. Constable
Department of Chemistry
University of Basel
Klingelbergstrasse 80, CH-4056 Basel, Switzerland

Dr. A. Braun
Hawaii Natural Energy Institute
School of Ocean and Earth Science and Technology
University of Hawaii at Manoa
402 Holmes Hall, 2540 Dole Street, Honolulu, HI 96822, USA

Dr. E. A. Rozhkova
Nano Bio Interfaces
Center for Nanoscale Materials
Argonne National Laboratory
9700 South Class Avenue, Argonne, IL, 60439, USA

Dr. K. Schrantz
University of Szeged
Department of Inorganic and Analytical Chemistry
Domtér7, H-6701 Szeged, Hungary

P. P. Wyss
FHNW – University of Applied Sciences Northwestern Switzerland
School of Life Sciences and Institute for Chemistry and Bioanalytics
Grüdenstrasse 40, CH-4132 Muttenz, Switzerland

Prof. T. Graule
Technische Universität Bergakademie Freiberg
Bernhard-v.-cotta Str.2, D-09596 Freiberg, Germany

DOI: 10.1002/adfm.201101830

the photovoltaic activity of a photosystem-I-based self-assembled monolayer[9] and the interaction of biomolecular assemblies with photo-electrochemical cells[10] has been provided recently. Following this approach, several systems have been developed, such as chloroplast photo-electrochemical cells,[11] chlorophyll-lecithin mixed-monolayer-coated electrodes, with the aim of designing solar-conversion systems based on the photosynthetic primary reactions,[12] photoelectrolysis at a chlorophyll-water-aggregate-coated platinum electrode as a photocathode,[13] immobilization of the bacterial photosynthetic-reaction center from *Rhodopseudomonas sphaeroides* on an SnO_2 electrode for photo-electrochemial conversion,[14] photo-electrochemical cells with chloroplast membranes, chloroplasts, photosystem-I particles, and purple membrane fragments containing bacteriorhodopsin,[15–18] to name a few.

In the present work, we show how the integration of light-harvesting biomolecules, such as C-phycocyanin on hematite, is a working method to increase the photocurrent by harvesting more photons.

The low band-gap energy of hematite (2.2 eV) allows the conversion of up to 40% of the incident solar radiation and, thus, makes it insofar suitable for photo-electrochemical cells; its abundance and its environmentally benign nature make it attractive for industrial applications.[19–21] Phycocyanin is the light-harvesting protein from the phycobilisome family, found in photosynthetic blue-green algae (cyanobacteria), red algae and the cryptomonads. It absorbs light from the red part of the visible spectrum (620 nm) and then provides a highly efficient exciton migration until the energy arrives at a photochemical reaction center through a funneling mechanism. It belongs to the oligomeric proteins, which use linear tetrapyrrole chromophores (phycocyanobilins) for light harvesting. The bilins are covalently attached to cysteine residues of the apoprotein by thioether bonds, and are not associated with metal ions.[22] The sensitization of hematite with a porphyrin derivatives can increase performance by harvesting incident photons with a higher efficiency.[23] The general viability of this route has been demonstrated recently, where phycocyanin has been used to sensitize the surface of TiO_2, which provides electron transfer from the photoexcited phycocyanin to the conduction band of the TiO_2.[24]

We can enhance the photocurrent from nanostructured hematite thin films by integrating the light-harvesting membrane protein, C-phycocyanin. This is accomplished by the immobilization of the protein on the hematite surface by both electrostatic and covalent surface functionalization, involving separation by a carbohydrate polymer such as agarose with a functional imidazole carbamate in activated form. A similar strategy of covalent functionalization has been adopted for immobilizing enzymes on silica-coated maghemite nanoparticles (γ-Fe_2O_3).[25] A different set of functionalization strategies has been developed for conjugating protease enzymes on magnetic nanoparticles.[26] Based on the same principle, a nanohybrid material was fabricated by the covalent functionalization of porphyrin on carbon nanohorns for the study of the photoinduced electrons and the energy-transfer process.[27] The rationale for using surface functionalization is the stabilization of the anchored protein and also the enforcement of the lateral cross-coupling between the proteins.

By this approach we expect a higher number density of immobilized proteins on the surface of the hematite. This will enable an extra portion of the light from the long-wavelength region of the solar spectrum to be harvested, and, therefore, assists in acquiring the enhanced optical properties of hematite thin-film electrodes, which will finally yield a higher photocurrent. In the next step, different properties of the hybrid system will be studied in order to assess their effects on the final performance.

2. Results and Discussion

Before we turn to the results of our investigation, we outline in detail the basic architecture of the essential components of our system and explain their expected functionality.

2.1. Surface Functionalization of Hematite Thin Films with C-Phycocyanin Protein

It has been established that when the pH of the surrounding environment of a material is below the pI, then the surface of the particular material becomes positively charged, or vice versa.[28] In the electrostatic conjugation process, the hematite surface became polarized as a result of the pH of the phosphate buffered saline (PBS) (7.4) being quite below the isoelectric point (pI) of hematite (8.4–8.5).[29] Similarly, the phycocyanin to be adsorbed on the hematite film was dissolved in a PBS buffer. The pI of phycocyanin is 4.64.[30] In this case, the surface charge of the phycocyanin will be negative, since the pH of the surrounding environment is higher than that of pI. Under such conditions, phycocyanin will be adsorbed on the hematite by simple electrostatic interactions, and not by chemical bonding. The conjugation is explained in **Scheme 1**A. After this, a thin layer of agarose was spin-coated onto it, so that the adsorbed phycocyanin on the hematite could be kept under stable conditions, from the structural and functional points of view. This will assist in the integrity of the system upon further chemical modification. The bioprotective properties of agarose, a sugar, can cause the phycocyanin to be stabilized by slowing down the molecular motion of the protein responsible for folding at ambient temperature.[31] In the next step, carbonyl di-imidazole (CDI) reacted with the hydroxyl-terminated agarose surface to create a reactive imidazole carbamate intermediate[32] that then coupled with the incoming amine-containing phycocyanin, finally resulting in an integrated system. CDI is an active carbonylating agent that contains two acylimidazole leaving groups. The chemistry underlying the above conjugation process is depicted in Scheme 1B. The active intermediate formed by the reaction of CDI with an OH group is an imidazolyl carbamate. Imidazole is released on attack by the amine, but the carbonyl group remains intact. In this way, hydroxyl-containing molecules can be coupled to molecules containing $-NH_2$ functional groups with the result of a one-carbon spacer, forming stable urethane (*N*-alkyl carbamate) linkages. This coupling procedure has, for example, been adopted for the activation of agarose beads for the biospecific affinity-based chromatographic isolation of serum antibodies.[33] CDI was thus used as a spacer

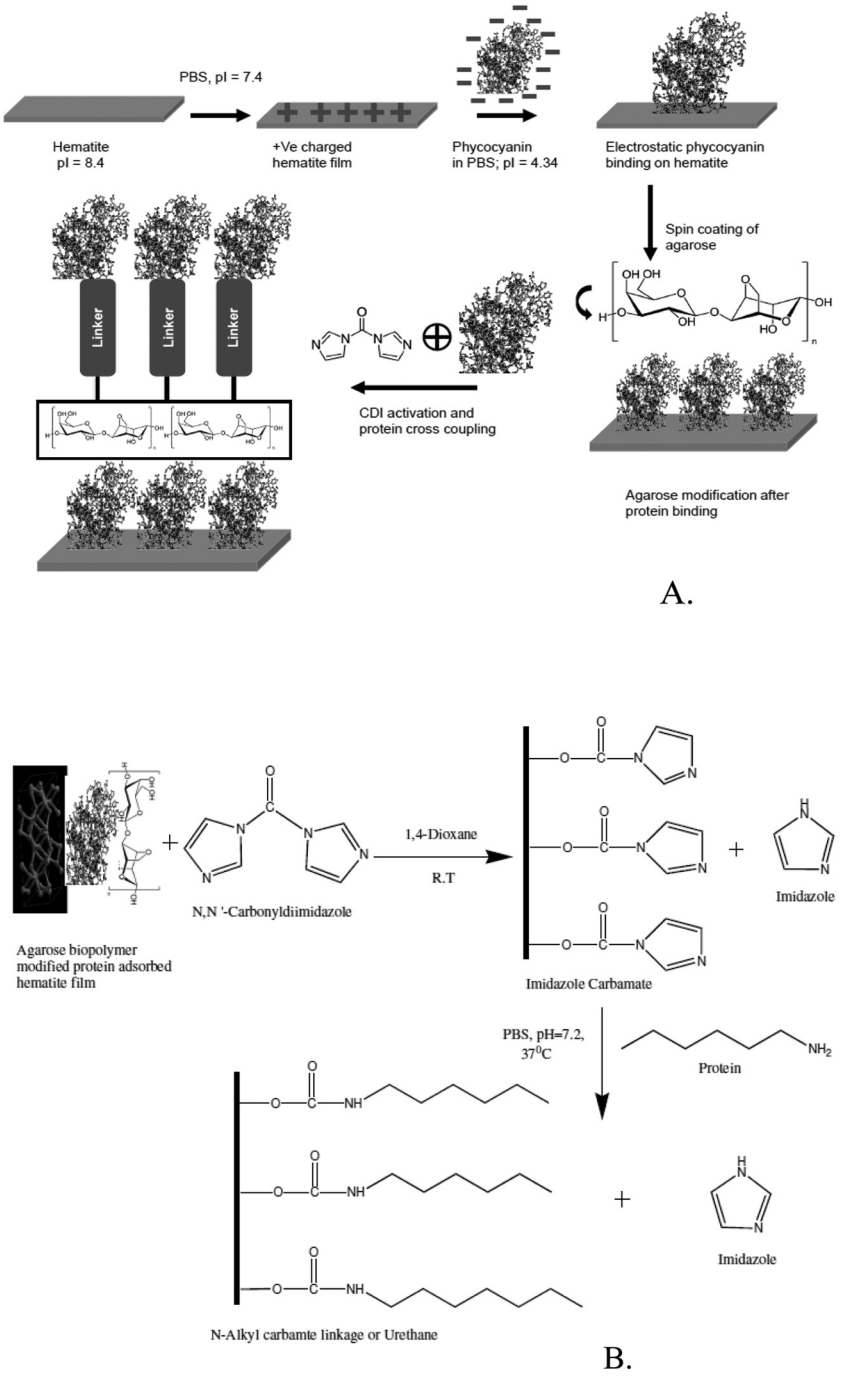

Scheme 1. A) Schematic of the conjugation strategy for the fabrication of the hematite–phycocyanin conjugate. B) The underlying chemistry in the above conjugation process.

arm to control the distance or separate the final, coupled protein from the hematite surface. This can allow for a specific coupling of the protein by avoiding steric hindrance between it and the immobilization support, such as, in this case, with the hematite film. An ideal spacer arm should have a bifunctional group to react with both the substrate and ligands, and it also helps in the placing of ligands at a suitable distance from the surface of the support.[34]

Now that we have explained the anticipated interaction of the functional components during the conjugation reaction, we present the experimental support. In order to be able to clearly correlate the structural, optical and photo-electrochemical properties with functionality, measurements were carried out on the same sample after stepwise modification from pristine hematite to hematite with the covalently linked protein. In order to check for the stability of the protein on the substrate surface (fluorine-doped tin oxide (FTO)) alone, we carried out chronoamperometric (current versus time) studies for 1 h under light conditions.

2.1.1. Probing the Conjugation Reaction Using Fourier Transform IR (FTIR) Spectroscopy

The immobilization and activation of phycocyanin in the covalently coupling system was confirmed by the analysis of FTIR-spectroscopy data. The FTIR spectra of all of the samples, A–B3, are shown in **Figure 1**. It should be noted that, in the case of agarose modification of the hematite film (B1), we directly spin-coated an agarose layer on the hematite without any additional phycocyanin layer. The spectrum, A, in the case of pristine hematite, shows an absorption band at 1736 cm^{-1} corresponding to the C=O stretching of an ester formed on the surface of the pristine film. This peak is prominent in all of the spectra from A–B2, except for B3. In spectrum B1, the characteristic bands of the agarose structure can be seen at 1455 and 1420 cm^{-1} and are assigned to –OH in plane bending and to $–CH_2$ symmetric bending, respectively.[34] The next bands at 1160 and 1060 cm^{-1} show the fingerprint of the carbohydrate cycle, and correspond to C–O–C asymmetric stretching and C–O stretching, respectively. The band at 1635 cm^{-1} corresponds to the OH bending mode of water absorbed on the agarose. Next, in the spectrum of the CDI-activated film (B2), we noticed an emerging band at around 1660 cm^{-1}, which is assigned to C=N stretching modes of the imidazole heterocycle from the imidazole carbamate intermediate formed during the activation step. The absorption bands at 1606, 1458 and 1420 cm^{-1} originate from the –NH bending vibration of the imidazole leaving group and the –CH stretching vibration of the imidazole heterocycle. The other bands at 1327, 1224 and 1123 cm^{-1} originate from the C–N stretching vibration in the active intermediate. In the final spectrum of the phycocyanin-conjugated hematite film (B3), the absence of a peak at 1660 cm^{-1} and the emergence of new bands at 1708 and 1606 cm^{-1}[35,36] corresponds to the C=O (amide-I band) and the –NH bending vibration. This confirms

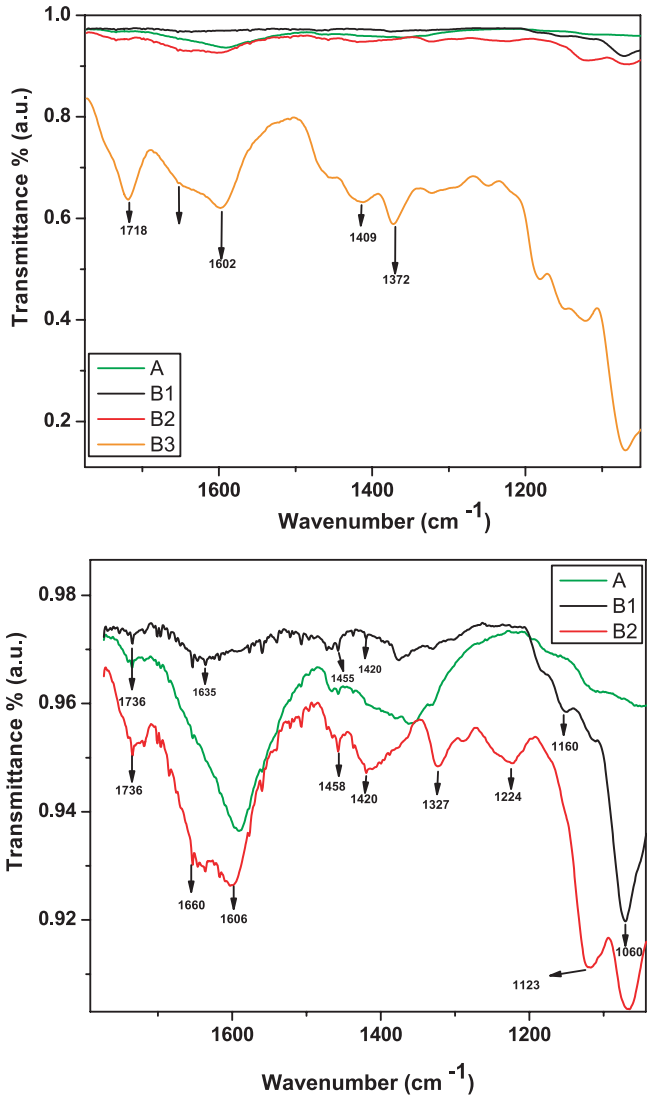

Figure 1. The FTIR spectra of the hematite–phycocyanin conjugate, along with pristine, agarose-modified and CDI-activated films, to probe the conjugation process.

the formation of stable urethane (*N*-alkyl carbamate) linkages formed by the condensation reaction between the imidazole ester and the amino functional group of the phycocyanin protein.

2.2. Structural Properties of the Hematite–Phycocyanin System

In order to learn about the potential influence of the surface modification on the structural properties of the hematite, we investigated a pristine hematite film and corresponding stepwise-modified films by X-ray diffractometry (XRD) (see **Figure 2**a). The diffractogram of the pristine hematite film (A) shows the substrate Bragg reflections (FTO substrate) as being the most-intense ones. Besides these, the two prominent hematite (104) and (110) Bragg reflections are observed, along with much-weaker reflections corresponding to the (012), (113), (024), (122), (310) and (1010) planes. This picture is well matched by XRD results of Si-doped hematite films synthesized by atmospheric-pressure chemical vapor deposition (CVD).[37] The XRD of the surface-modified films from B and B1–B3 showed interesting results when we closely inspected the peak intensities of the (104) and (110) reflections, along with the (101) reflection from the substrate, shown in Figure 2b. For the protein-adsorbed film (B), we found that the (104)-reflection intensity increased, whereas the (110)-reflection intensity decreased in comparison with those for the pristine film. Upon addition of agarose (B1), the intensity reached a maximum and the intensity of the (110) reflection increased with respect to that of B1; again, the (104)-reflection intensity decreased after CDI activation (B2), while the intensity of the (110) reflection remained the same as that for B and B1. Finally, upon the cross-coupling of another protein molecule, the same peak intensity remained, as in the case of the CDI-activated film. In all cases, the peaks were getting sharper, which was well justified by calculating the crystallite size. We quantified this trend using the Scherrer equation[38] and the crystallite sizes are plotted in Figure 2c. There, we noticed that the crystallite size increased from the pristine (A) to the phycocyanin-conjugated (B3) film. The growing crystallite size may be attributed to the erosion of the nanoparticle surface in the film by the organics used for the modification. Such an erosion phenomenon is not uncommon and has been observed on protein-functionalized porous-silicon surfaces.[39] Due to the increasing amount of organic content on the pristine hematite film, the overall thickness of the film might increase to some extent. The erosion can have a noticeable effect on the differences in the XRD peak intensity and the photoabsorptive ability of the hematite film. To validate this, we looked into the relative Bragg peak intensity ratio ($I_{(104)}/I_{(101)}$) from the hematite and the substrate part, as shown in Figure 2d. The Bragg peak ratio changed at each surface-modification step. On careful inspection of the expanded views of the (104) and (101) peak intensities from the hematite and the substrate, we found that the substrate peak intensity varied slightly for the films after each surface-modification step. We looked into the preferential growth of the hematite crystal plane after each surface-modification step. It is known that the hematite (001) plane plays an important role in the catalytic activity and in electronic conductivity,[40] which has a further influence on the observed photocurrent. In this case, the change of the relative Bragg peak ratio ($I_{(104)}/I_{(110)}$) gives an account of the crystallographically preferred growth of hematite and is shown in Figure 2e. By careful inspection of the trend, we found that both planes grew equally with respect to each other. This trend followed similarly to $I_{(104)}/I_{(101)}$, which was due to the change in the overall thickness of the pristine hematite film, as discussed above. This means that both planes grew equally in each surface-modification step. This validates that the there was no preferred growth of the hematite crystalline lattice upon the integration of the protein and also that the photocurrent observed did not fit with the trend.

2.3. Optical Properties of the Hematite–Phycocyanin System

In view of the effect of the light-harvesting protein (C-phycocyanin) on the optical properties of hematite, we analyzed the

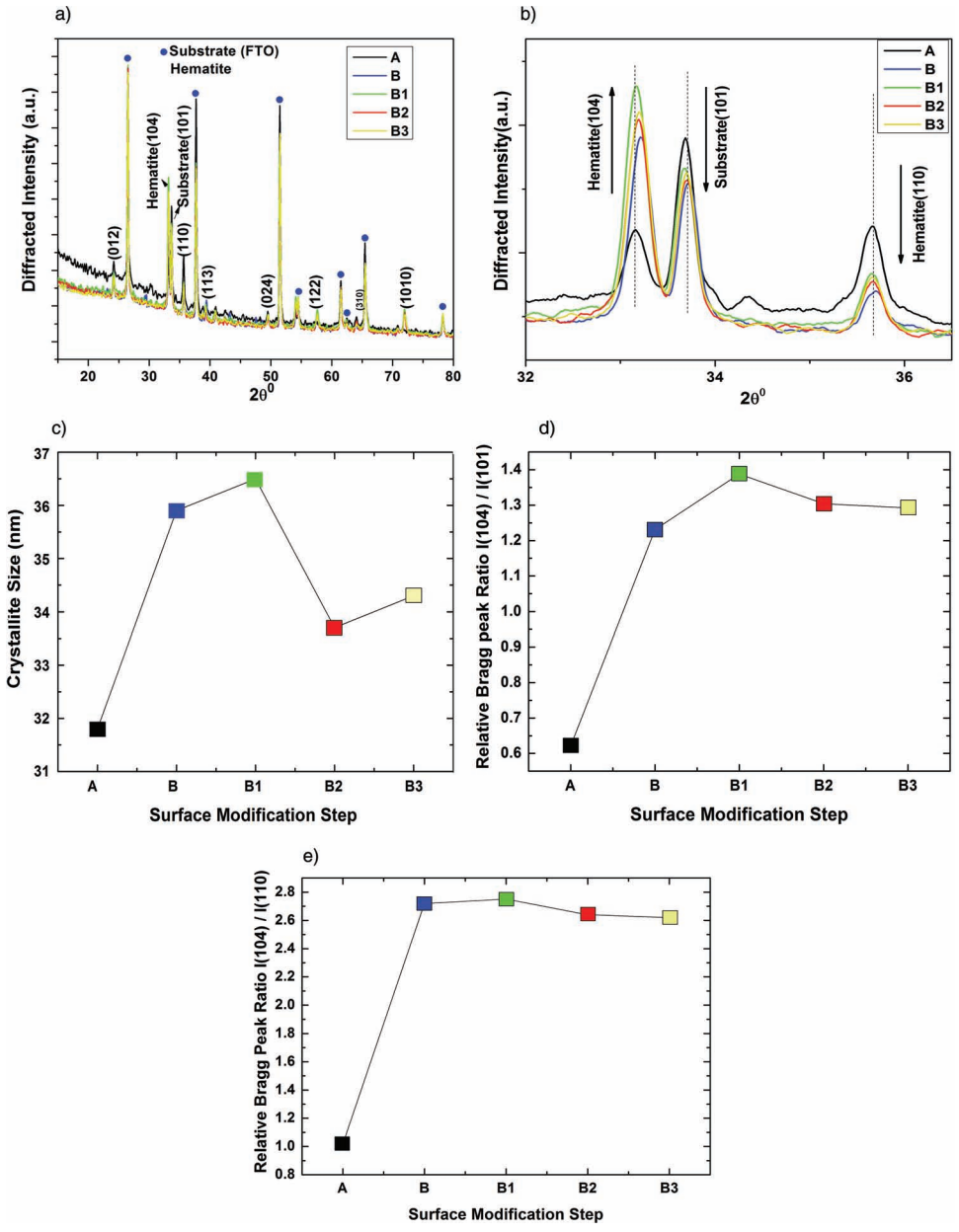

Figure 2. a) The X-ray diffractogram of pristine hematite (A), phycocyanin adsorbed on hematite (B), agarose coated (B1), CDI activated (B2) and phycocyanin conjugated (B3) films. b) Expanded view of the (104) and (110) reflections, along with the (101) reflection from the substrate. c) The crystallite-size variation of the hematite after surface modification, calculated using the Scherrer equation. d) Variation in the relative Bragg peak intensity ratio ($I_{(104)}/I_{(101)}$) from the hematite and the substrate to see the effect of thickness. e) Relative Bragg peak ratio ($I_{(104)}/I_{(110)}$) of hematite and its variation at each surface-modification step.

UV–vis spectra of the pristine and other films after each surface-modification step. Generally, the photocurrent obtained from hematite depends mainly on the quantity of absorbed photons that are converted into electrical energy by the generation of electron-hole excitons. The anticipated enhanced photocurrent obtained in this case could be related to the light-harvesting action of the protein molecules that absorb in the red part of the visible spectrum. This means that, by integrating this protein on the hematite or photoactive layer, we can increase the light-absorbing properties by taking advantage of the extended region of visible wavelengths. For example, there are several factors that can affect the total number of photons absorbed by a solar cell's active layer. These are: an optical absorption comparable to the solar spectrum, the absorptivity, and the broadening of the absorption-wavelength range. In our proposed system, hematite is the photoactive layer and the generation of a photocurrent in this case will be enhanced only when the total number of photons absorbed by it increases.

This is only possible when the absorption range and absorption peak value or the intensity increases for hematite. Therefore, by anchoring the C-phycocyanin molecule on the hematite surface, the absorption peak value can be increased with a broadening of the spectral range. This was done by functionalization of the hematite surface with C-phycocyanin, as described above. The absorption spectra (**Figure 3**a) of all of the films from A–B3 reveal that the pristine hematite film (A) absorbed at 404 nm, 444 nm and 545 nm, which corresponds to the usual band positions of bulk hematite.[41] The band at 444 nm appeared due to ligand field transition and that at 545 nm is the absorption edge of the hematite. In the next step, on adsorbing protein on the hematite surface (B), spectral broadening occurred, with the 444 nm band shifted towards longer wavelengths, while the other band at 404 nm remained at the same position. We noticed also that the intensity of the absorption edge or peak absorption value was increasing. We can attribute the change of the spectral weight to the interaction of the absorbed protein on the hematite surface, and the enhancement in the peak absorption value occurred due to the extra portion of light absorbed by the protein. C-phycocyanin absorbs at 620 nm, which is the standard absorbance wavelength supported by another study,[42] and this can be seen from the inset to Figure 3a. A change in the absorption maximum of phycocyanin was observed on interaction with the nanoparticles from the film. This change was originally proposed to be due to the perturbation of the surface-charge density of the nanoparticle and the protein,[43] which manifested in changing the absorption spectrum. In the next step of surface activation, on adding the agarose layer, the spectrum of B1 looked the same like that of B, with a slight decrease in the intensity of the 444 nm band. On further treatment with CDI, the spectra of the activated films (B2) changed slightly, with a consequent increase in the absorption-edge peak intensity. Also the 444 nm band position shifted to a longer wavelength, while the intensity remained the same, like that for spectra B and B1. This shift towards larger wavelength can be explained by the changes in particle size. This is already evident from the crystallite calculation shown in Figure 2c, whereby we found that the crystallite size varied with preceding surface modification. It was established that the crystallite size changed with changes in the Fe^{3+}–O^{2-} distance in the hematite due to temperature treatment. This resulted in a red shift of about 20 nm to shigher wavelengths for the absorption band due to the Fe^{3+} ligand field transition.[44] On conjugating with the final phycocyanin molecule, the intensity of the 444 nm band reached a maximum and again shifted to a shorter wavelength. This was also due to the variation in crystallite size as stated above. A similar behavior has been observed in the photoluminescence spectra of a porous-Si matrix, where the spectral shift was attributed to the erosion of the nanocrystalline Si by surface oxidation from the interacting protein.[39] The transmittance spectra (Figure 3b) further showed the photoabsorptive capability of the phycocyanin molecule in the conjugated system. Hereby, we looked into the transmittance of the modified film at 620 nm, where the phycocyanin absorbs photons. The inset to the figure shows that the transmittance decreased strongly on going from the pristine film to the phycocyanin cross-linked film. This further confirms that the cross-linked film absorbed more photons, which is obvious by considering the maximum

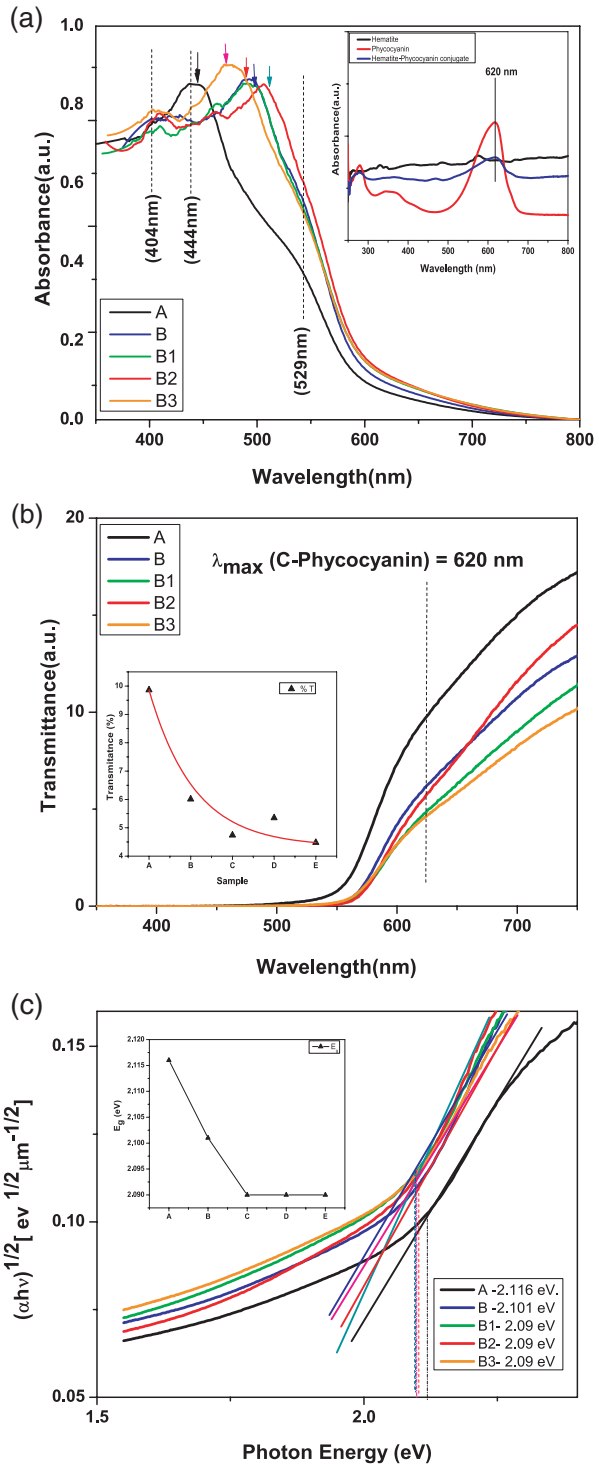

Figure 3. a) UV–vis absorption spectra of pristine hematite (A), phycocyanin adsorbed on hematite (B), and agarose-coated (B1), CDI-activated (B2) and phycocyanin-conjugated (B3) films. Inset: the change in the absorption maximum of phycocyanin on interacting with nanoparticles from the film. b) Transmittance spectra of films A–E. Inset: the variation of %T with surface-modification step. c) The energy band gap (E_g) of the pristine film after each surface-modification step in all of the films. The inset shows the trend in the variation of E_g.

absorption shown at 444 nm. To give an account of the changes in the electronic structure of the pristine hematite film, we determined the energy band gap (E_g) of the pristine film after each surface-modification step (Figure 3c). From here, we found that the band gap ranged at around 2.09–2.12 eV, which placed it in the band-gap energy of hematite (1.9–2.2 eV).[45] It followed the pattern depicted in the inset to Figure 3c. It slightly shifted with the modification step, but stabilized at 2.09 eV, when the agarose layer was added. From this, we conclude that the surface functionalization did not affect the electronic structure of the hematite. Nevertheless, by conjugating phycocyanin with hematite, the absorption intensity increased by the increase in the number of photons absorbed due to the light-harvesting action of the C-phycocyanin molecule. This, finally, enhanced the photocurrent of the hematite film, as observed from further analysis of the photo-electrochemical properties. A similar study has been made regarding the light harvesting and photocurrent of a P3HT:PCBM bulk-heterojunction solar cell by the contribution of coumarin 6 using optical spectroscopy.[46]

2.4. Probing the Integrity of the Protein Structure Using Raman Spectroscopy

We applied Raman spectromicroscopy to investigate the integrity of the protein structure in the final conjugated system. The objective of this part of the study was to probe the stability of the chromophore present inside the phycocyanin protein in the conjugated system, which, as will be shown in the next section, showed a significantly enhanced photocurrent. Generally, this chromophore is responsible for the light absorption and the energy-transfer mechanism towards the reaction center. The corresponding Raman spectra of the pristine and modified films, along with spectra from the bare protein deposited on glass and on the FTO substrate, are shown in **Figure 4**. The

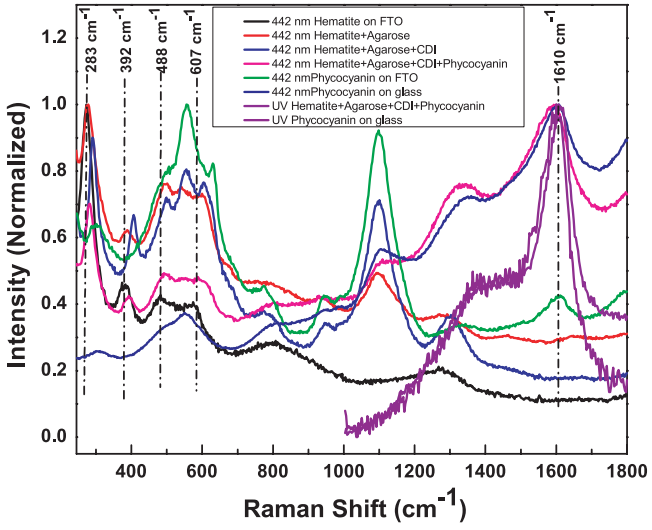

Figure 4. The Raman spectra of the pristine and modified films, along with spectra from the bare protein on glass and FTO substrates, excited by visible and UV light, show the integrity of the protein after electrochemical treatment.

Raman spectrum of pristine hematite on FTO shows four bands, at 283, 392, 488 and 607 cm^{-1}, with a slight shift from the reference spectra.[47] The band at 488 cm^{-1} was assigned to the A_{1g} mode and the remaining peaks were assigned to the E_g mode.[48] The weak intensity band observed above 600 cm^{-1} was mainly attributed to the presence of trace amounts of magnetite or maghemite with Raman forbidden transitions.[49] Upon addition of the agarose layer, we found that the intensities of all of the bands increased. This was due to the interaction of the Raman light with the density of the next incoming media. Furthermore, on activating the agarose-treated hematite films with carbonyl di-imidazole, a new band evolved in between 488 and 607 cm^{-1} and the peaks from the hematite film exhibited a blue shift. This blue shift could be due to the decrease in crystallite size during the respective modification step, as is evident from Figure 2c and is consistent with earlier studies on TiO_2 powders and thin films.[50] Finally, on conjugating the phycocyanin protein with the activated film, the Raman spectrum showed a new band at around 1610 cm^{-1} that fits well with the phycobiliprotein (the protein chromophore) band around 1597 cm^{-1} in the Raman spectrum of C-phycocyanin excited at 488 nm.[51] In the spectra obtained from the bare phycocyanin on FTO and glass substrates, this band was also observed at 1610 cm^{-1}. Consideration of this scenario allows us to state that the protein chromophore structure remained in a stable configuration. On the other hand, if the structure were to be destroyed by denaturation, then the band would gradually lose its intensity. However, it remained the same, as is evident from the spectra. In addition, we used UV excitation to probe the spectra of the phycocyanin on glass and of the protein-conjugated system, as shown in Figure 4. Since the sample contained a strong chromophore, UV excitation was also preferable to visible excitation, because the Raman excitation gets obscured by the fluorescence of the chromophore in the latter case. Here, we also observed the same band at 1610 cm^{-1} and the intensity of the band remained the same in both cases. From these discussions, we propose that the structure of the chromophore inside the phycocyanin protein remains intact after finally conjugating over the hematite surface.

2.5. Photo-electrochemical Properties of the Hematite–Phycocyanin System

The photo-electrochemical performance of the hematite–phycocyanin integrated system was obtained by sweeping current–potential (I–V) scans in a 1 M KOH electrolyte (pH = 13.6) in the dark and under simulated solar illumination (AM 1.5), as shown in **Figure 5**a. Initially, the saturated photocurrent density of the pristine hematite sample (A) was 281.40 μA cm^{-2}, which began at an onset potential of –100 mV and increased until the dark current onset began at 450 mV. After adding the first phycocyanin layer (B), the photocurrent density increased to 420.26 μA cm^{-2} and remained constant on adding the agarose layer (B1). After the activation process by CDI (D), it increased up to a value of 458.76 μA cm^{-2} and finally reached 491.53 μA cm^{-2} after conjugation of the next phycocyanin layer (E), as depicted in Scheme 1A. This means that after integrating the final protein molecule by covalent cross-coupling,

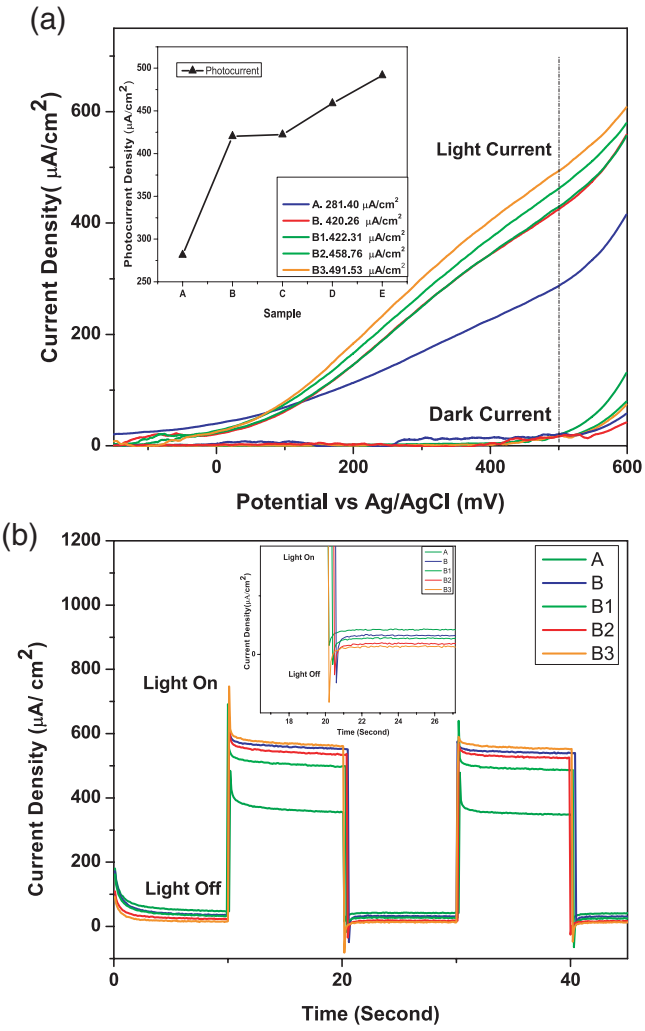

Figure 5. a) The photocurrent measured for pristine hematite (A), phycocyanin-adsorbed on hematite (B), agarose-coated (B1), CDI-activated (B2) and phycocyanin-conjugated (B3) films in a 1 M KOH electrolyte (pH = 13.6) with a three-electrode photo-electrochemical cell in the dark and under simulated solar illumination (AM 1.5). b) The photocurrent-transient responses of pristine hematite (A), phycocyanin-adsorbed on hematite (B), agarose-coated (B1), CDI-activated (B2) and phycocyanin-conjugated (B3) films measured during chronoamperometric cycling of all electrodes.

we could increase the photocurrent by over 200 μA cm^{-2}. We attribute this virtually two-fold increase in photocurrent to the extra light-absorbing capability of the hematite film assisted by the light-harvesting property of the phycocyanin. This corresponds to the changes in the absorption spectrum of the hematite–phycocyanin conjugate, as discussed above. To get a clear insight into the same, we have performed IPCE (incident-photon-to-electron conversion efficiency) studies of the pristine hematite film (A), the phycocyanin-adsorbed hematite film (B), the agarose-modified phycocyanin-adsorbed hematite (B1) and the conjugated film (B2) (**Figure 6**f). From this, it can be clearly observed that the efficiency of the protein-functionalized film was enhanced at 620 nm, which is the absorption maximum of the phycocyanin molecule, whereas the pristine hematite film did not show any enhanced efficiency at 600–620 nm. The inset clearly demonstrates that the photocurrent was enhanced by the functionalization of the pristine hematite film by the phycocyanin in both the adsorbed (B) and conjugated steps (B3). This clearly shows also that the light absorbed by the phycocyanin directly caused the increase in the photocurrent. A similar rise in photocurrent efficiency has been observed in the dye sensitization of hematite nanorods, whereby an improvement of the photocurrent efficiency is reached by red shifting the photocurrent onset at 750 nm, with a maximum of 699 nm.[52] Besides these, there may be some other factors that can enhance the photocurrent, such as the photodynamic action of phycocyanin and the effect of carbon oxidation.

2.5.1. Possible Factors Influencing the Increase in Photocurrent

Phycocyanin has a good photodynamic action for water photooxidation. It can interact with water molecules (solvent) or with hematite (substrate) by a so-called type-I mechanism, whereby it transfers charge to the solvent (electrolyte in this case) with the generation of radicals.[53] This happens only when phycocyanin gets excited with light. Photosensitized oxidations are the basis for photodynamic action. The first step of this photodynamic action is the absorption of light by a sensitizer (sens) to produce an excited state (sens*). In this case, the phycocyanin acts as the sensitizer. In the presence of oxygen, two competing reactions of the excited-state sensitizer can occur, which are, respectively, Type-I and Type-II mechanisms. Hydroxyl radicals ($OH^{\bullet}$) can be generated by the following mechanism when C-phycocyanin is irradiated with visible light (470 nm). It is speculated that in our case, the sens* can either react with the hematite surface or with the electrolyte during photoelectrochemical operation (Type I) or with oxygen (Type II). One important question that arises from the functionalization of the hematite is that of charge transport across the components of the film assembly. Consequently, we carried out a photocurrent-transient response study (Figure 5b), which was done by chopping the light during the chronoamperometric operation of the electrode at a constant potential of 600 mV. The photocurrent of the protein-adsorbed film (B) and the conjugated film (B3) were higher than that of the pristine film (A). On turning the light on, we obtained photocurrent-transient spikes in the upward direction, which then decayed from a peak to a steady state (A–B3). On turning the light off after 10 s of illumination, the current dropped towards zero and reverted back again when the light was turned back on. This falling photocurrent-transient decay is indicative of a more-rapid removal of conduction-band electrons into the bulk[54] and the spike-like transient response is caused by a "back reaction", or a recombination of the photogenerated electrons and holes with the surface states.[55] The falling transient[56] is rationalized in terms of photogeneration of an $OH^{\bullet}$ radical, which acts as an electron acceptor. Assuming the charge-transfer mechanism to prevail, if we carefully look into the cathodic transient spike (inset of Figure 5b) for each of the samples, we find that, in case of the phycocyanin cross-linked system, the current decays slowly to a steady state, in comparison with other samples. This has been accounted in the energy-band diagram given by Kathiravan

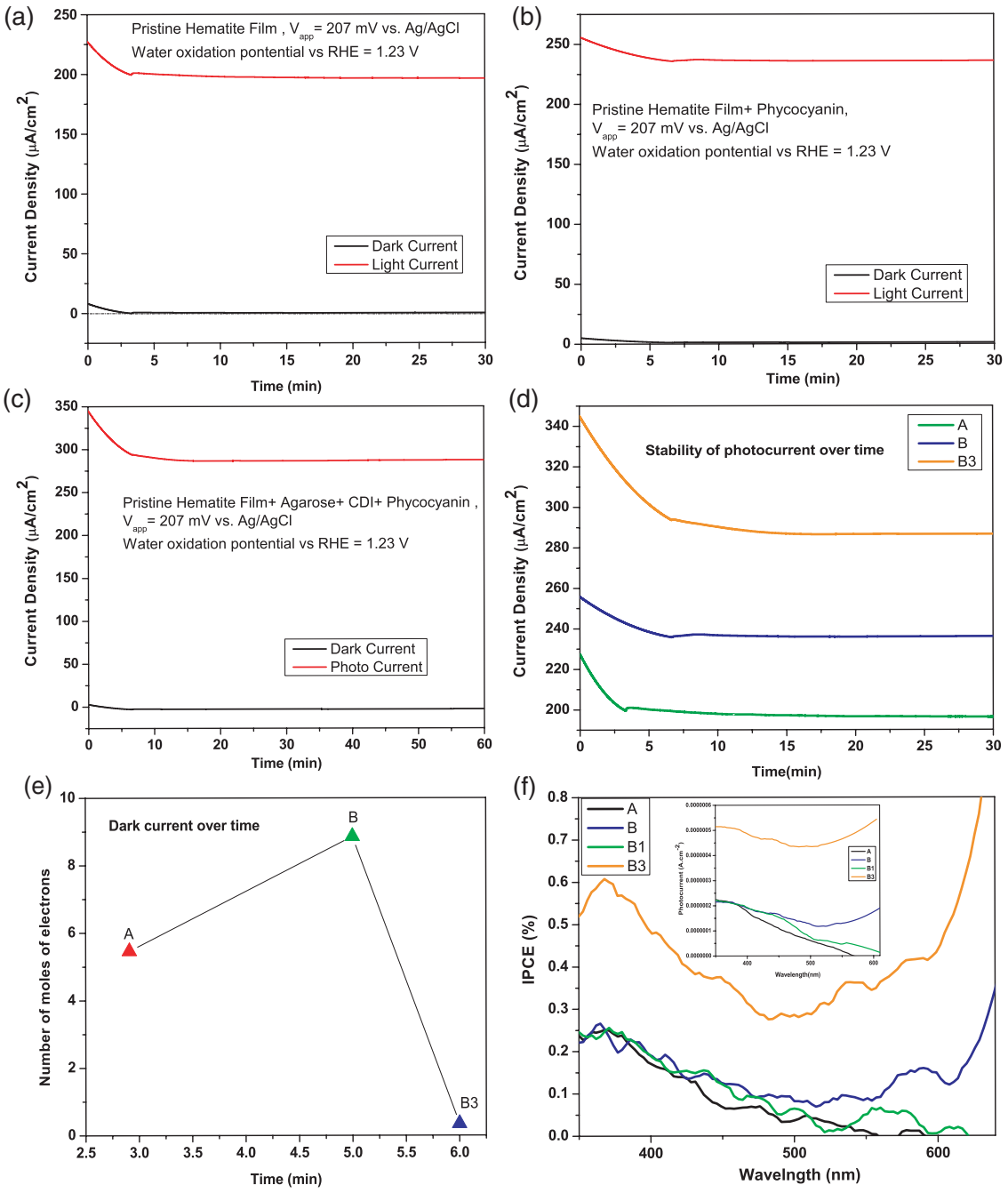

Figure 6. a–c) Long-term sustainability study of the photocurrent by carrying out the chronoamperometric measurement of the hematite film (a) and the protein functionalized films (b and c) at the oxidation potentials of water (207 mV, 1.23 V vs. RHE). d) The stability of the photocurrent over time for the pristine and protein-functionalized films. e) Number of moles of electrons obtained during a dark chronoamperometric scan after 10 min of operation for samples A, B and B3. f) IPCE measurement of pristine hematite film (A), phycocyanin-absorbed hematite film (B), agarose-modified phycocyanin-adsorbed hematite (B1) and conjugated film (B3).

and Renganathans,[24] which we adopt here for the reader in **Scheme 2**. The magnitude of this cathodic transient spike was quite high in the case of the protein-conjugated film. It is evident that, during the chopped chronoamperometric measurement, when the light was turned off, OH• at the surface continued to scavenge conduction-band electrons and created a cathodic transient spike until the OH• was consumed. On the other hand, the current transients in the positive direction represent the accumulation of holes at the electrode/electrolyte interface under the light condition. The increase in the magnitude of cathodic transient spike in the hematite–phycocyanin cross-linking step, as shown in the inset of Figure 5b, suggests

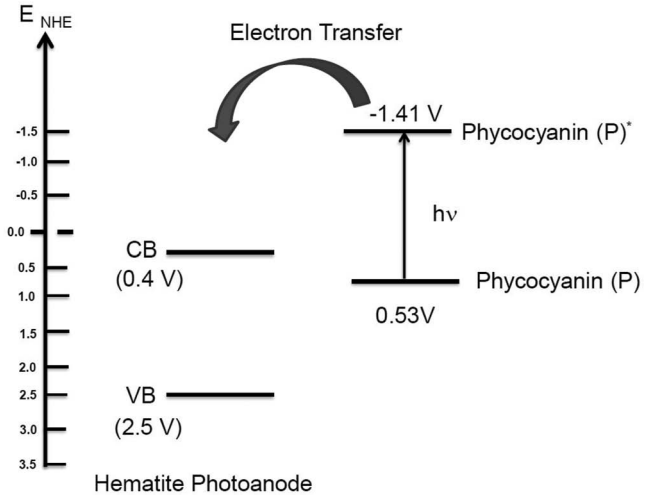

Scheme 2. Energy-band diagram showing the charge transfer from the excited-state phycocyanin to the conduction band of the hematite.

that more OH• were produced on the hematite surface due to extra photodynamic action of the phycocyanin, or that it took more time for the conduction-band electrons to consume all of the radicals. Dotan et al.[57] recently showed the effect of a hole scavenger such as H_2O_2 on the photo-electrochemical properties of hematite. It was found that when H_2O_2 is added to the electrolyte, the current transients disappear and purely faradic photocurrents are obtained. The absence of current transients suggests that no charge is accumulated at the electrode/electrolyte interface. This indicates that all of the charges that reach the interface are injected to the electrolyte or consumed by a very-fast surface recombination.

2.5.2. Source of the Enhanced Photocurrent in the Hematite–Phycocyanin System

The photocurrent ideally originates from water oxidation by the photogenerated holes. Parasitic contributions may come from other oxidative processes, such as from the oxidation of organics, like protein or non-converted volatile precursor components, on the electrode surface, which, over time, may be fully consumed. To test this, we performed long-term chronoamperometry of the hematite film (A) and the functionalized film (B and B3) at the oxidation potentials of water (207 mV, 1.23 V versus a reversible hydrogen electrode (RHE)) for a suitable period of time. Here, we found reasonable stability in the photocurrent of the protein-functionalized film. Upon careful analysis of the chronoamperometry results (Figure 6a–c), we found that the dark-current magnitudes were fairly low. It was noted that during the first couple of minutes, the dark current decayed quickly with time. We calculated the total number of moles of electrons generated after 5 min of each chronoamperometric operation during dark and light experiments using a procedure described by Bora et al.[58] The number of moles of electrons obtained and the corresponding number of moles of oxygen evolved in each case are presented in **Table 1**. The stability of the photocurrent over time is plotted in Figure 6d.

Table 1. The number of moles of electrons obtained and the corresponding number of moles of oxygen evolved, calculated from the chronoamperometric measurements.

Sample	Condition	Number of moles of electrons	Number of moles of oxygen
A	Dark	9.55 nmol	2.38 nmol
	Light	3.83 µmol	0.957 µmol
B	Dark	29.3 nmol	7.33 nmol
	Light	4.58 µmol	1.145 µmol
B3	Dark	42.21 nmol	10.56 nmol
	Light	5.47 µmol	1.371 µmol

We can clearly see that the protein-functionalized film shows a sustained enhanced current, as was obtained during the *I–V* scan (Figure 5a). We plotted the number of moles of electrons obtained during the dark chronoamperometric scan after 10 min of operation for samples A, B and B3 (Figure 6e). It was observed that the number of moles of electrons resulting from the dark oxidation of organic material decreased to a lower value over the period of time. Interestingly, in the protein-conjugated hematite film (B3) this value was negligible. This clearly signifies that the enhanced photocurrent of the protein-functionalized film did not originate from the oxidation of the protein itself. The origin of the enhanced photocurrent was thus from water photo-oxidation and the extra light harvesting of the phycocyanin at 620 nm, evident from the IPCE result (Figure 6f).

2.5.3. Comparison with Other Light-Harvesting/Water-Oxidation Hybrid Systems

Hybrid systems for energy generation have been developed before, such as the TiO_2-nanotube–bacteriorhodopsin hybrid system,[59] a biomimetic light-harvesting device composed of columnar TiO_2 film and chlorosomes[7] and a self-assembled monolayer of a light-harvesting complex on amino-terminated indium tin oxide (ITO).[60]

In the biomimetic light-harvesting device, the chlorosomes were sprayed on the dye-adsorbed TiO_2. The device performance was based on enhanced current generation due to the interaction of the dye and the chlorosomes over the entire wavelength region. The photocurrent increased remarkably in the device containing chlorosomes in the long-wavelength region, from 640 nm to the near-infrared. The presence of chlorosomes in the device increased the photocurrent by over a factor of 30.

In the case of the TiO_2-nanotube–bacteriorhodopsin hybrid system, under AM 1.5 illumination, the photocurrent density of the hybrid electrode was found to be around 50% over pure TiO_2 nanotube. A redox electrolyte increased the photocurrent value to 0.87 mA cm^{-2}. The system showed a slight increase in photocurrent, similar to the hematite–phycocyanin system in our case. This increase was attributed to a continuous proton-pumping mechanism over the extended illumination time.

For the hybrid device consisting of a self-assembled monolayer of the light-harvesting complex (LHC) on amino-terminated ITO, the photocurrent responses showed a maximum at the wavelength corresponding to the absorption

band of the complex when the LHC and the reaction centre were combined. Upon illumination at 880 nm the enhanced photocurrent was observed. However, in the case of the LHC alone, the photocurrent was mainly generated by the light absorbed at 770 nm. Again, if just the reaction center was immobilized on amino-terminated ITO, a photocurrent was not observed at 880 nm.

The enhanced photocurrent observed at 880 nm in the assembled LH1/RC-core complex (light harvesting complex 1/reaction center) can be ascribed to energy transfer from LH1 to RC and then electron transfer from the electrode to the RC. This indicates that the LH1/RC-core complex was well organized on the ITO and the photocurrents were driven by light that was initially absorbed by the light-harvesting component.

2.5.4. Role of Phycocyanin in Enhancing the Photocurrent and Long-Term Operational Stability

To investigate the individual role of phycocyanin in enhancing the photocurrent, we studied the transient photoresponse of the phycocyanin-adsorbed FTO substrate and pristine FTO by applying a potential of 100 mV during chronoamperometric operation (**Figure 7**a) as a control experiment. Here, phycocyanin was first transferred to the FTO by dipping the FTO into a 2×10^{-6} M solution of phycocyanin. We followed, for this particular case, a protocol presented by Janzen and Seibert in 1980,[14] because they too worked on tin oxide substrates. An excess amount of phycocyanin solution was removed from the lower part of the FTO and dried in the dark. The FTO with adsorbed phycocyanin showed a higher photocurrent than the pristine FTO. This further validates the role of phycocyanin in enhancing the photocurrent on the integration of the hematite electrode. Similar observations were made on the LH1-RC complex on an APS (3-aminopropyltriethoxysilane)-terminated ITO electrode.[60] During the light-on condition, we observed a photocurrent-transient spike when the phycocyanin was adsorbed on the FTO, which was absent in the case of pristine one. The reason behind the absence of any transient photocurrent spikes[61] in the case of the pristine FTO is the limitation to the charge-transport process by recombination in the bulk. Sivula et al.[62] found a similar result in the case of thermal treatment of a mesoporous hematite film, whereby they considered the transient spike at the photocurrent-onset potential. The stability of phycocyanin on FTO was studied in a control experiment with chronoamperometry for 1 h under light conditions, as shown in Figure 7b. The phycocyanin showed good operational stability and had an increased photocurrent in comparison with bare FTO.

To further check the functionality of the species B after electrochemical treatment, we recorded the absorbance spectra of species B. The difference spectrum (Figure S4, Supporting Information) was obtained by subtracting the pristine hematite spectrum from the absorbance of species B in the wavelength range from 400 nm to 700 nm. We found a significant absorbance even after electrochemical treatment up to 600 mV. The spectral signature coincided with that from phycoerythrin.[63] This, together with comparison with the spectrum of phycocyanin 645[22] confirms that species B has the spectral signature from phycocyanin.

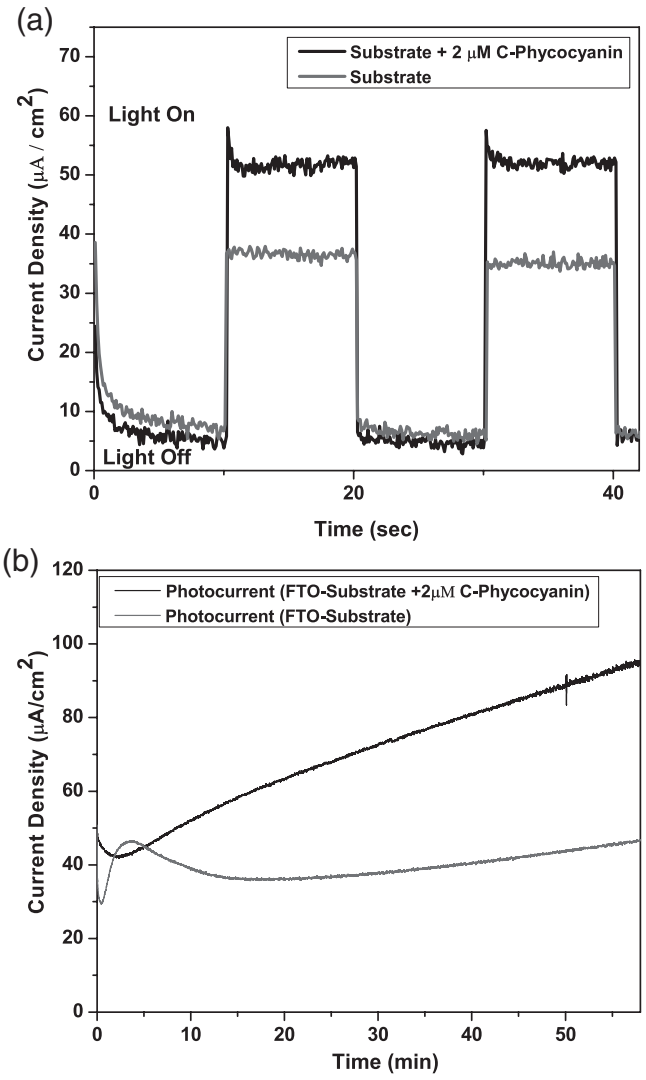

Figure 7. a) Transient photoresponse of the phycocyanin-adsorbed FTO substrate and pristine FTO during chronoamperometric cycling to evaluate the individual role of the phycocyanin protein in providing extra photocurrent. b) Long-term stability measurement of the phycocyanin chronoamperometrically for 1 h under light conditions.

With respect to scale-up and large-scale production of phycocyanin-based devices, a new protein-separation technique called expanded-bed adsorption chromatography (EBAC) could, in the future, lower the cost of extraction and purification.[64]

3. Conclusions

We have developed a strategy for increasing the photocurrent of a hematite thin-film electrode by integrating C-phycocyanin protein with a linker-mediated covalent cross-coupling technique. The hematite structure is preserved, as is evident from XRD. UV spectra show increased optical absorption by the harvesting of more photons on final coupling with protein. This helps further in getting an enhanced photocurrent in the chemically cross-linked system, in comparison with pristine hematite.

Transient studies show an enhanced photoresponse of the protein-coupled hematite system. Enhanced cathodic transient spikes in the hematite–phycocyanin cross-linking step allow us to speculate that more OH radicals may be produced on the hematite surface due to the enhanced photodynamic action of the phycocyanin. From long-term sustainability studies of the functionalized photoelectrode, it is shown that the enhanced photocurrent of the protein-functionalized film does not originate from the oxidation of the protein itself. The origin of the enhanced photocurrent is indeed from water photo-oxidation and the extra light-harvesting action of the phycocyanin at 620 nm, as is evident from IPCE result.

4. Experimental Section

Materials: The iron nitrate nonahydrate, oleic acid and tetrahydrofuran (THF) used in the synthesis of the hematite were of reagent grade (Sigma–Aldrich). The solvents used for the functionalization were anhydrous toluene and 1,4-dioxane, and PBS was used as the coupling buffer. The films were deposited on FTO glass (Hardford Glass Inc.). The protein used was C-phycocyanin isolated from *Spirulina* sp. (Sigma–Aldrich, Switzerland, 99.9% purity). The linker used for the conjugation of the C-phycocyanin with hematite was 1,1'-CDI (Sigma–Aldrich, Switzerland, reagent grade 99.9% purity).

Synthesis of Hematite Thin Films and Immobilization of C-Phycocyanin on Hematite by Electrostatic and Covalent Surface Functionalization: Pristine hematite thin films (A) were synthesized using a previously adopted method.[65] For the synthesis of the conjugated protein–hematite system by electrostatic interactions (B) of differently charged species, the hematite films were kept for 2 h in 0.5 M PBS, so as to obtain a positively charged surface. The PBS solution was prepared by mixing subtle amounts of NaCl, KH_2PO_4 and Na_2HPO_4 so as to get the requisite concentration. Furthermore, a 200 µl solution of C-phycocyanin was dispersed over the hematite surface using a pipette and kept for 12 h overnight in the dark at ambient temperature. The solution was prepared by dissolving suitable amounts of C-phycocyanin in PBS buffer (pH=7.2) to get the desired concentration. In the preparation of the hematite–C-phycocyanin conjugates by covalent cross-coupling, the hematite film readily adsorbed with protein solution (B) was subjected to spin-coating of an agarose layer (B1) in order to decorate the surface with free hydroxyl groups. The agarose solution was prepared by dissolving 1 mg of agarose powder in 100 ml of double-distilled water by heating at 60–70 °C and using a magnetic stirrer. After this, the film was allowed to dry at room temperature prior to CDI activation (B2). For the CDI treatment of the agarose-treated protein-coated hematite film (B1), firstly 50 mg ml^{-1} (0.3×10^{-3} M) of CDI was dissolved in 5 ml of dioxane and the agarose-modified electrodes (B1) were immersed in the respective solutions for 2 h at room temperature. When the reaction was completed, the hematite/protein/agarose assembly was considered as an *activated electrode* (B2) and was rinsed 3 times with anhydrous toluene to remove excess CDI and reaction by-products. The *activated electrode* (B2) was then treated with a 0.5 M PBS solution having pH = 7.4. The pH of the coupling buffer determined the greater reactivity of the imidazole carbamate and greater coupling yields for the protein. Then, activated electrodes were reacted with 200×10^{-6} M C-phycocyanin (B3) for 3 h at 37 °C on a hot plate with magnetic stirrer. After the conjugation reaction, the electrodes were rinsed with washing buffer (0.01 M PBS), pH = 7.2, to remove unbound protein molecules.

Materials Characterization: The conjugate formation by covalent surface functionalization was studied using attenuated-total-reflection (ATR)-FTIR spectrometry. The spectra were recorded using a Bio-Rad FTS 575C instrument equipped with a mercury cadmium telluride detector and a horizontal nine-reflection diamond ATR unit with KRS-5 optics (SensIR Technologies, Danbury, CT). The spectra were recorded from 400 to 4000 cm^{-1} at a 2 cm^{-1} resolution. The phase purity of the pristine and the phycocyanin-conjugated hematite films were further checked by XRD (PAN Analytical X'Pert PRO, Cu K_α radiation). The optical properties of the samples were studied using a UV–vis spectrometer (Carry Scan 50). The morphology and composition of the pristine and modified films were studied using a field-emission scanning electron microscope (FE-SEM) (Hitachi, S 4800) equipped with an energy-dispersive X-ray (EDX) detector (Oxford instruments) with an accelerating voltage of 15 keV. The surface morphology of the pristine hematite along with the conjugated film was studied by atomic force microscopy (AFM) in tapping mode, Nanosurf-AFM, (Mobile S). The optical Raman spectra were recorded using a Renishaw inVia Raman Microscope, using a blue laser at 442 nm (exposure time of 10.0 s, laser power 100%). For characterizing the protein samples alone, we used a UV excitation at 325 nm (exposure time 50.0 s, 4 accumulations at 100% laser power).

Photo-electrochemical Characterization: The photocurrent spectra were recorded using a Voltalab potentiostat in a three-electrode configuration with 1 M KOH (pH = 13.6) as the electrolyte, Ag/AgCl/sat. KCl as the reference electrode and a platinum counterelectrode. In all cases, the maximum applied potential was 600 mV. The photo-electrochemical cell was custom built from polyether ether ketone (PEEK) plastic. The pristine hematite electrode (A), along with the modified ones (B–B3), was illuminated on a 0.45 cm^2 area of electrolyte and a fused silica window with a 0.5 cm^2 circular mask; the total geometric area immersed in the electrolyte was approximately 2.6 cm^2. Sunlight was simulated using a filtered xenon lamp from LOT Oriel, with the light intensity adjusted to AM 1.5. The transient photoresponse for the samples was studied by chopping the light during the chronoamperometric (current versus time) measurement, with the working electrode kept constant at 600 mV and the current measured against the time. Photocurrent action spectra were taken in a custom-built IPCE set-up operated by Lab View. The spectra were obtained under a 300 W Xe lamp connected with a monochromator (LOT). The wavelength was scanned at 2 nm s^{-1} and the applied voltage was 0 mV versus a saturated calomel electrode (SCE) in the aforementioned cell. The monochromatic photocurrent of pristine hematite film versus the different wavelengths (300–700 nm) was obtained by loading the power-calibration data in the Lab View software. This was firstly measured using a Si photodiode with a power meter (Thor Labs) before starting the IPCE measurement.

Supporting Information

Supporting Information is available from the Wiley Online Library or from the author.

Acknowledgements

Funding for this research was provided by the Swiss Federal Office of Energy project No. 100411, the Seventh Framework Program "Novel Materials for Energy Applications" grant No. 227179 (NanoPEC – Nanostructured Photoelectrodes for Energy Conversion), the Swiss National Science Foundation R'Equip No. 206021-121306 and IZK0Z2-133944. The spectro-electrochemical cell was built by Peter Wyss and Marc Zollinger (Empa Machine Shop) after a design provided by Laboratory for Photonics and Interfaces, EPFL Lausanne. The IPCE instrument was built by Dr. Fabio La Mattina and Andre Kupferschmid, Empa.

Received: August 8, 2011
Revised: September 27, 2011
Published online: December 12, 2011

[1] N. S. Lewis, *Nature* **2001**, *414*, 589.
[2] A. Fujishima, K. Honda, *Nature* **1972**, *238*, 37.
[3] R. Das, P. J. Kiley, M. Segal, J. Norville, A. A. Yu, L. Wang, S. A. Trammell, L. E. Reddick, R. Kumar, F. Stellacci, N. Lebedev,

J. B. Schnur, D. Bruce, S. Zhang, M. Baldo, *Nano Lett.* **2004**, *4*, 1079.
[4] I. Ron, L. Sepunaru, S. Itzhakov, T. Belenkova, N. Friedman, I. Pecht, M. Sheves, D. Cahen, *J. Am. Chem. Soc.* **2010**, *132*, 4131.
[5] N. P. Reynolds, S. Janusz, M. Escalante-Marun, J. Timney, R. E. Ducker, J. D. Olsen, C. Otto, V. Subramaniam, G. J. Leggett, C. N. Hunter, *J. Am. Chem. Soc.* **2007**, *129*, 14625.
[6] N. Khare, C. M. Eggleston, D. M. Lovelace, S. W. Boese, *J.Colloid Interface Sci.* **2006**, *303*, 404.
[7] L. B. Modesto-Lopez, E. J. Thimsen, A. M. Collins, R. E. Blankenship, P. Biswas, *Energy Environ. Sci.* **2010**, *3*, 216.
[8] P. N. Ciesielski, A. M. Scott, C. J. Faulkner, B. J. Berron, D. E. Cliffel, G. K. Jennings, *ACS Nano* **2008**, *2*, 2465.
[9] I. Carmeli, L. Frolov, C. Carmeli, S. Richter, *J. Am. Chem. Soc.* **2007**, *129*, 12352.
[10] M. Grätzel, *Nature* **2001**, *414*, 338.
[11] R. Bhardwaj, R. L. Pan, E. L. Gross, *Nature* **1981**, *289*, 396.
[12] T. Miyasaka, T. Watanabe, *Nature* **1979**, *277*, 638.
[13] F. K. Fong, N. Winograd, *J. Am. Chem. Soc.* **1976**, *98*, 2287.
[14] A. F. Janzen, M. Seibert, *Nature* **1980**, *286*, 584.
[15] *Living Systems as an Energy Converter: Proc. Eur. Conf. on Living Systems as Energy Converters*, (Eds: R. Buvet, M. J. Allen, J. P. Massué), North-Holland, Amsterdam, The Netherlands **1977**.
[16] H. Ochiai, H. Shibata, A. Fujishima, K. Honda, *Agricultural Biol. Chem. Tokyo* **1979**, *43*, 181.
[17] E. L. Gross, D. R. Youngman, S. L. Winemiller, *Photochem. Photobiol.* **1978**, *28*, 249.
[18] V. P. Skulachev, *FEBS Lett.* **1976**, *64*, 23.
[19] A. Duret, M. Grätzel, *J. Phys. Chem. B* **2005**, *109*, 17184.
[20] A. A. Tahir, K. G. U. Wijayantha, S. Saremi-Yarahmadi, M. Mazhar, V. McKee, *Chem. Mater.* **2009**, *21*, 3763.
[21] R. L. Spray, K. Choi, *Chem. Mater.* **2009**, *21*, 3701.
[22] D. S. Berns, R. McColl, *Chem. Rev.* **1989**, *89*, 807.
[23] F. V. Herrera, P. Grez, R. Schrebler, L. A. Ballesteros, E. Munoz, R. Cordova, H. Altamirano, E. A. Dalchiele, *J. Electrochem. Soc.* **2010**, *157*, 302.
[24] A. Kathiravan, R. Renganathans, *J. Colloid Interface Sci.* **2009**, *335*, 196.
[25] M. I. Shukoor, F. Natalio, H. A. Therese, M. N. Tahir, V. Ksenofontov, M. Panthofer, M. Eberhardt, P. Theato, H. C. Schroder, W. E. G. Muller, W. Tremel, *Chem. Mater.* **2008**, *20*, 3567.
[26] D. Li, W. Y. Teoh, J. J. Gooding, C. Selomulya, R. Amal, *Adv. Funct. Mater.* **2010**, *20*, 1767.
[27] G. Pagona, A. S. D. Sandanayaka, Y. Araki, J. Fan, N. Tagmatarchis, G. Charalambidis, A. G. Coutsolelos, B. Boitrel, M. Yudasaka, S. Iijima, O. Ito, *Adv. Funct. Mater.* **2007**, *17*, 1705.
[28] G. D. Parfit, *Pure Appl. Chem.* **1976**, *48*, 415.
[29] M. Kosmulski, *Chemical Properties of Material Surfaces*, Marcel Dekker, Inc., New York USA **2001**.
[30] S. M. Adams, O. H. W. Kao, D. S. Berns, *Plant Physiol.* **1979**, *64*, 525.
[31] I. Köper, S. Combet, W. Petry, M. C. Bellissent-Funel, *Eur. Biophys. J.* **2008**, *37*, 739.
[32] G. T. Hermanson, *Bioconjugate Techniques*, 2nd ed., Academic Press, London United Kingdom **2008**.
[33] M. T. W. Hearn, E. L. Harris, G. S. Bethell, W. S. Hancock, J. A. Ayers, *J. Chromatogr.* **1981**, *218*, 509.
[34] H. Zou, Q. Luo, D. Zhou, *J. Biochem. Biophys. Methods* **2001**, *49*, 199.
[35] S. A. Alila, M. Ferraria, A. M. Botelho do Rego, S. Boufi, *Carbohydr. Polym.* **2009**, *77*, 553.
[36] H. Günzler, H. Gremlich, *IR Spectroscopy*, Wiley-VCH, Weinheim, Germany **2002**.
[37] A. Kay, I. Cesar, M. Grätzel, *J. Am. Chem. Soc.* **2006**, *128*, 15714.
[38] A. L. Patterson, *Phys. Rev.* **1939**, *56*, 978.
[39] L. Tay, N. L. Rowell, D. J. Lockwood, R. Boukherroub, *J. Vac. Sci. Technol. A* **2006**, *24*, 747.
[40] O. Warschkow, D. E. Ellis, J. Hwang, N. Mansourian-Hadavi, T. O. Mason, *J. Am. Ceram. Soc.* **2002**, *85*, 213.
[41] R. M. Cornell, U. Schwertmann, *The Iron Oxides – Structure, Properties, Reactions, Occurrence and Uses*, Wiley-VCH, Weinheim Germany **1996**.
[42] B. Soni, B. Kalavadia, U. Trivedi, D. Madamwar, *Process Biochem.* **2006**, *41*, 2017.
[43] T. Pradeep, *Nano: The Essentials*, Tata McGraw Hill, India **2007**.
[44] T. B. Saito, *Chem. Soc. Jpn.* **1965**, *38*, 2008.
[45] J. H. Kennedy, K. W. Frese, *J. Electrochem. Soc.* **1978**, *125*, 709.
[46] Y. A. M. Ismail, T. Soga, T. Jimbo, *Sol. Energy Mater. Sol. Cells* **2010**, *94*, 1406.
[47] E. Grant, *Ann. Rev. Plant Physiol.* **1981**, *32*, 327.
[48] A. M. Jubb, H. C. Allen, *ACS Appl. Mater. Interfaces* **2010**, *2*, 2804.
[49] I. Chamritski, G. Burns, *J. Phys. Chem. B* **2005**, *109*, 4965.
[50] W. F. Zhang, Y. L. He, M. S. Zhang, Z. Yin, Q. Chen, *J. Phys. D: Appl. Phys.* **2000**, *33*, 912.
[51] M. Debreczeny, Z. Gombos, B. Szalontai, *Eur. Biophys. J.* **1992**, *21*, 193.
[52] N. Beermann, L. Vayssieres, S. E. Lindquist, A. Hegfeldt, *J. Electrochem. Soc.* **2000**, *147*, 2456.
[53] S. Zhang, J. Xie, J. Zhang, J. Zhao, L. Jiang, *Biochim. Biophys. Acta.* **1999**, *1426*,205.
[54] C. M. Eggleston, A. J. A. Shankle, A. J. Moyer, I. Cesar, M. Grätzel, *Aquatic Sci.* **2009**, *71*, 151.
[55] A. Watanabe, H. Kozuka, *J. Phys. Chem. B.* **2003**, *107*, 12713.
[56] K. L. Hardee, A. J. Bard, *J. Electrochem. Soc.* **1977**, *124*, 215.
[57] H. Dotan, K. Sivula, M. Grätzel, A. Rothschild, S. C Warren, *Energy Environ. Sci.* **2011**, *4*, 958.
[58] D. K. Bora, A. Braun, R. Erni, G. Fortunato, T. Graule, E. C. Constable, *Chem. Mater.* **2011**, *23*, 2051.
[59] N. K. Allam, C.-W. Yen, R. D. Near, M. A. El-Sayad, *Energy Environ. Sci.* **2011**, *4*, 2909.
[60] Y. Suemori, M. Nagata, Y. Nakamura, K. Nakagawa, A. Okuda, J. Inagaki, K. Shinohara, M. Ogawa, K. Iida, T. Dewa, K. Yamashita, A. Gardiner, R. J. Cogdell, M. Nango, *Photosynth. Res.* **2006**, *90*, 17.
[61] C. Sanchez, K. D. Sieber, G. A. Somorjai, *J. Electroanal. Chem.* **1988**, *252*, 269.
[62] K. Sivula, R. Zboril, F. Le Formal, R. Robert, A. Weidenkaff, J. Tucek, J. Frydrych, M. Grätzel, *J. Am. Chem. Soc.* **2010**, *132*, 7436.
[63] J. M. Berg, J. L. Tymoczko, L. Stryer, *Biochemistry*, 5th ed., W. H. Freeman, New York USA **2002**.
[64] A. Ramos, F. G. Acién, J. M. Fernández-Sevilla, C. V. González, R. Bermejo, *J. Chem. Technol. Biotechnol.* **2010**, *85*, 783.
[65] D. K. Bora, A. Braun, S. Erat, A. K. Ariffin, R. Löhnert, K. Sivula, R. Manhke, J. Töpfer, M. Gräzel, T. Graule, *J. Phys. Chem. C* **2011**, *115*, 5619.